Extended Date Figures

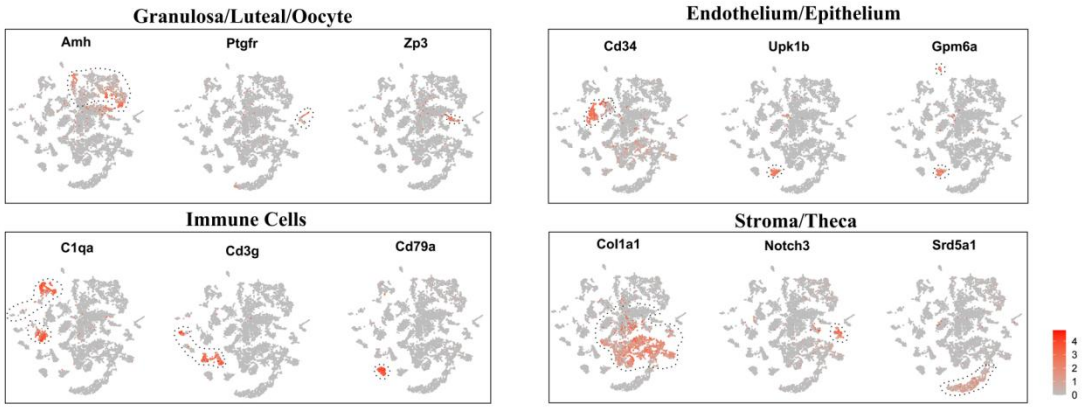

Extended Data Fig. 1|t-SNE plots illustrating the expression of mark genes in ovarian cells, with color denoting the level of expression.

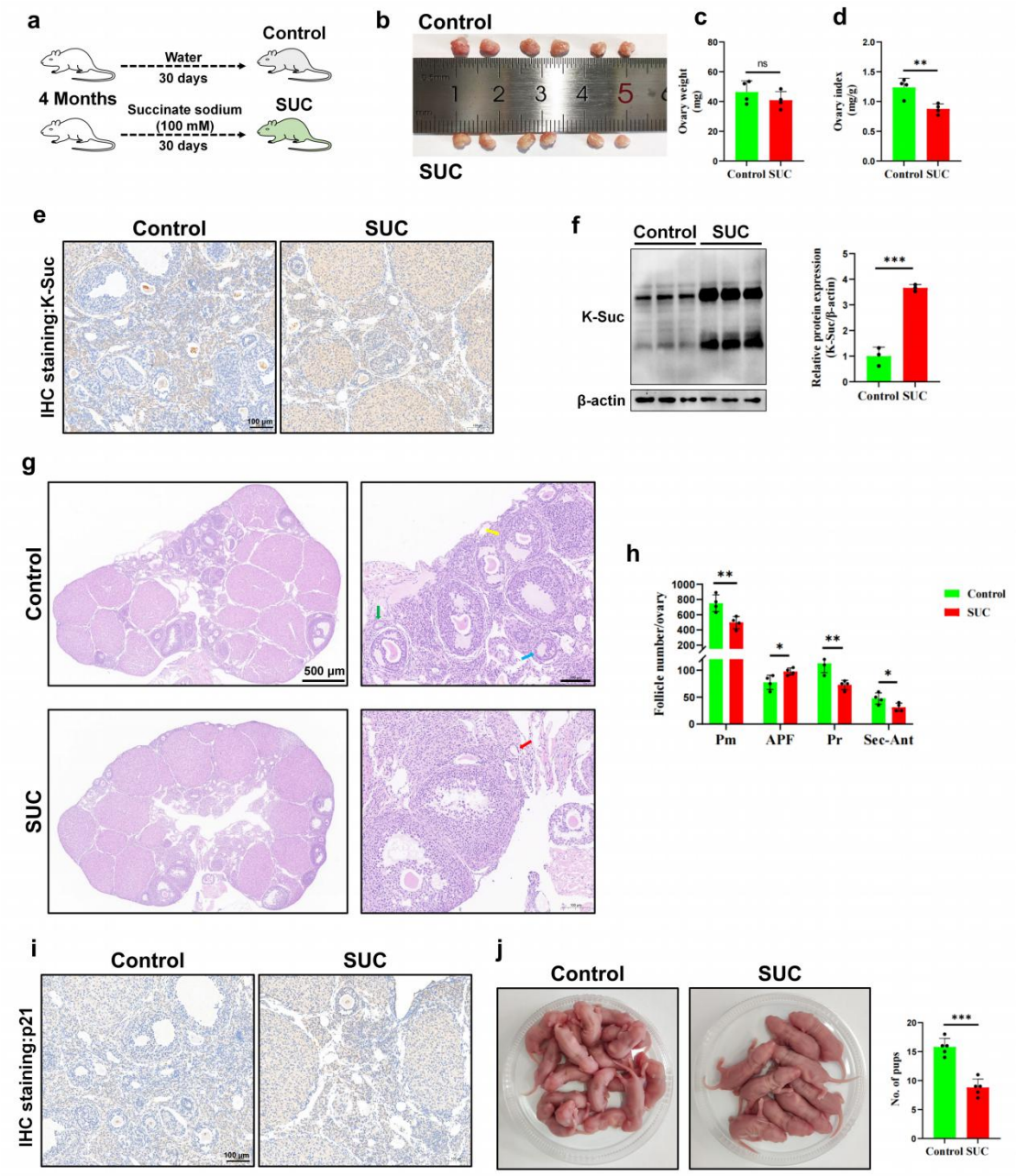

Extended Data Fig. 2|Excessive Ksuc accelerates mouse ovarian aging. **a**, Schematic showing continuous feeding of 4-month-old female mice with water and exogenous succinate sodium (100 mM) for 30 days. **b-d**, Images of the ovaries of female mice in the control group and SUC group were taken (**b**), and the ovary weight (**c**) and ovary index (ovary weight/body weight) (**d**) were measured. (n = 4 females per group). **e**, Representative IHC images of the ovaries of control and SUC female mice with anti-Succinylation (n = 4 per group). Scale bars, 100 μm. **f**, Lysine succinylation levels were determined by immunoblot in the ovaries of control and SUC female mice, and the quantifications were presented as mean ± SEM of three independent experiments. **g**, Follicles were classified into primordial (Pm, yellow arrows), activated primordial (APF: oocyte diameter greater than 20 μm without cuboidal granulosa cells, red arrows), primary (Pr, green arrows), or secondary-antral (Sec-Ant, blue arrows) stages. Scale bars, 500 μm and 100 μm. **h**, Quantification of the number of Follicular stages per ovary in the control and SUC groups. **i**, Representative IHC images of the ovaries of control and SUC female mice with anti-p21 (n= 4 per group). Scale bars, 100 μm. **j**, Mean pup numbers of Control and SUC mice. (n = 6 females per group). Statistical analysis was performed using unpaired, two-tailed Student's t test. $* P < 0.05$, $** P < 0.01$.

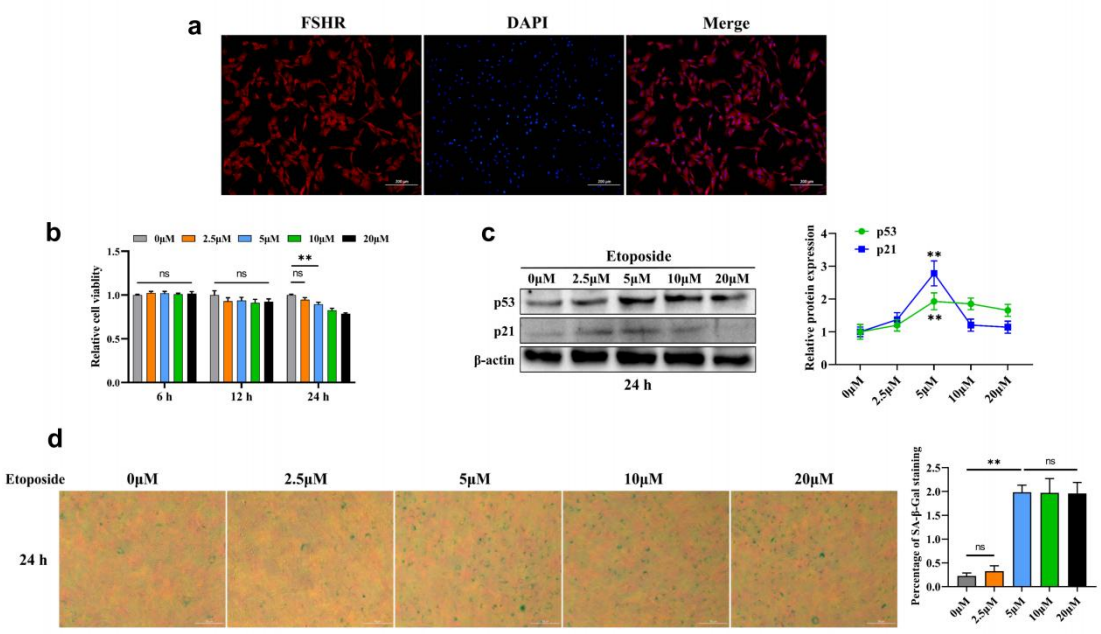

Extended Data Fig. 3|Etoposide induces senescence of ovarian GCs *in vitro*. a, GCs were identified by FSHR specific immunofluorescence staining. b, The effect of Etoposide on the viability of GCs was determined by CCK-8, and the quantifications were presented as mean ± SEM of five independent experiments. **c**, p53 and p21 protein levels were determined by immunoblot in GCs treated with different concentrations of Etoposide for 24 h, and the quantifications were presented as mean ± SEM of three independent experiments. **d**, The levels of β-galactosidase were determined in GCs after treated with different concentrations of Etoposide for 24 h, and the quantifications were presented as mean ± SEM of three independent experiments. Statistical analysis was performed using unpaired, two-tailed Student's t test. $* P < 0.05$, $** P < 0.01$.

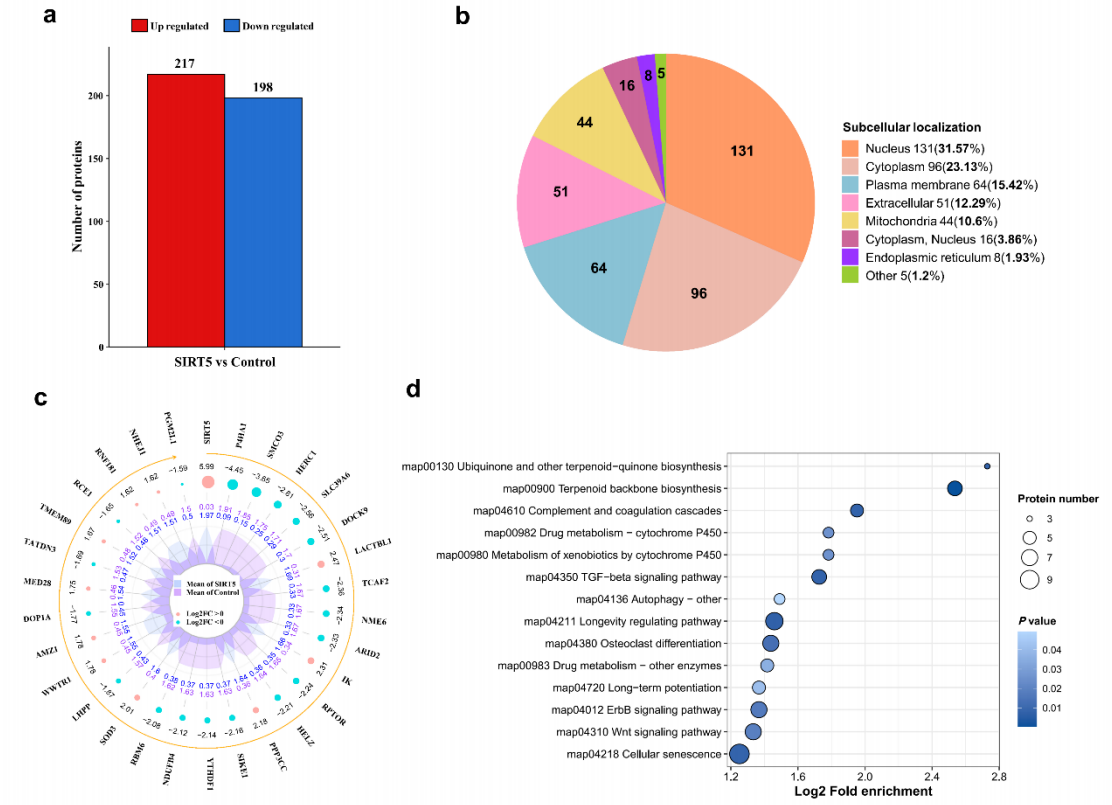

Extended Data Fig. 4|SIRT5 affects the protein expression of ovarian GCs. **a**, Statistical analysis differentially expressed proteins in 4D proteomics data. **b**, Subcellular structure types of differentially expressed proteins. Different colors represent the corresponding subcellular structure information, and the legend shows the name and

proportion of the corresponding species. **c**, Radar plot of relative expression levels of Top 30 differential expressed proteins in the two groups. The first circle represents the name of the differential protein. The second circle indicates that the absolute value of the difference protein Log_2 Fold change is sorted from large to small. The third circle represents the differential expression change Ratio value of the comparison group of Log_2 conversion. Pink indicates up-regulation, blue indicates down-regulation, and the larger point indicates the larger value. The fourth circle represents the average quantitative value of the two groups. **d**, KEGG pathway enrichment analysis of differentially expressed proteins in the two groups.

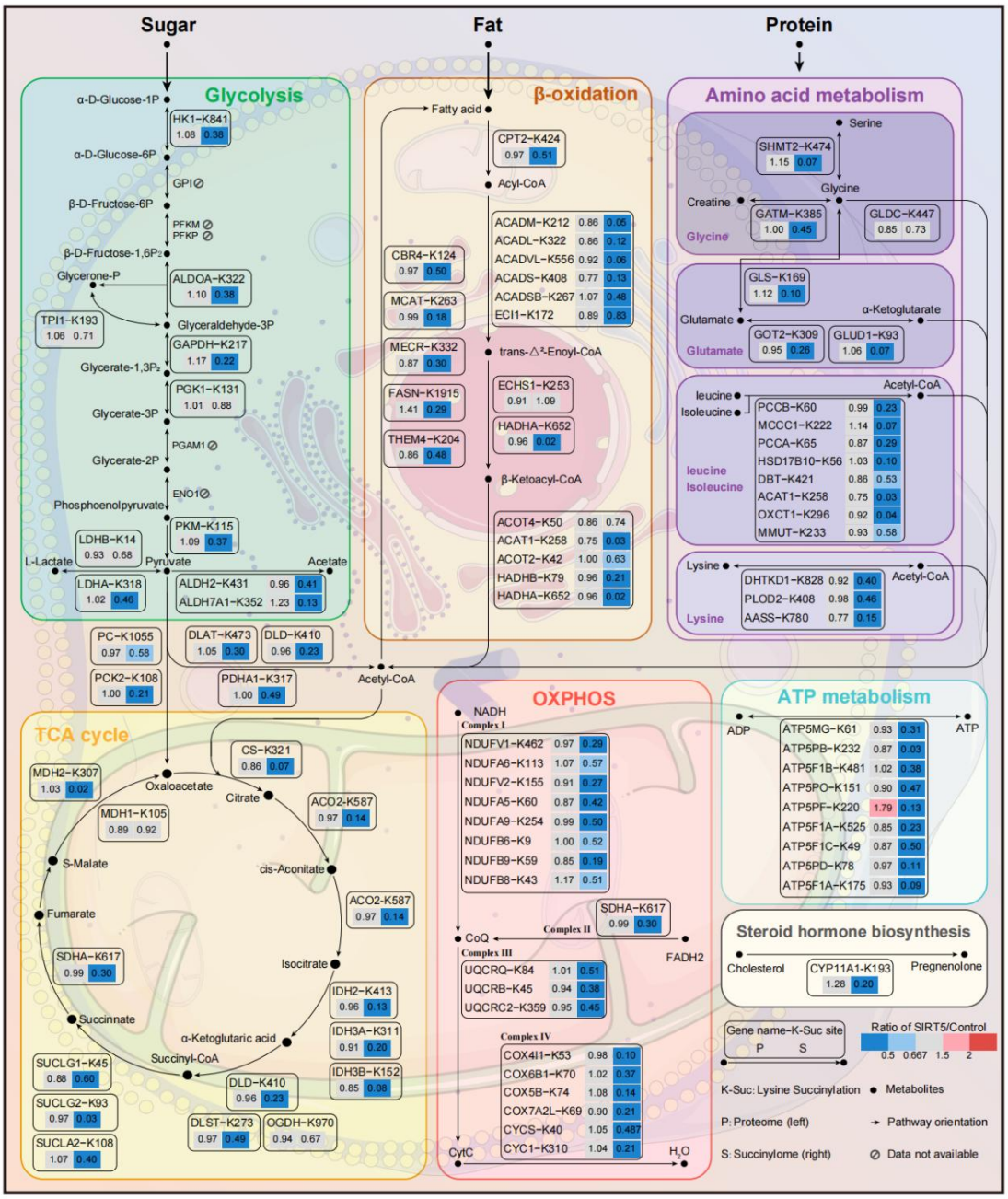

Extended Data Fig. 5|Panoramic overview of metabolic pathways based on 4D succinylation proteomics data.

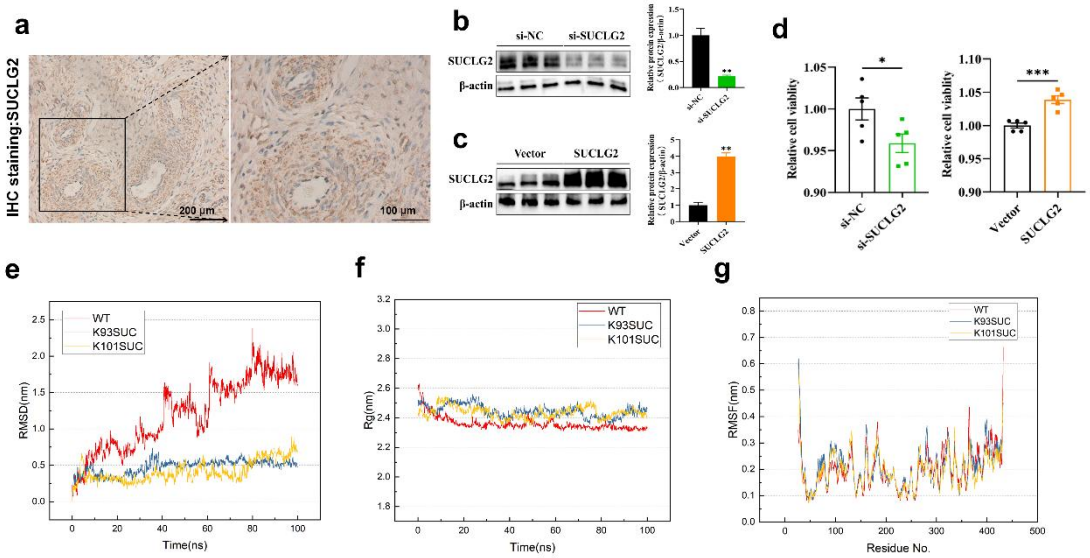

Extended Data Fig. 6|SUCLG2 influences the viability of GCs, and the succinylation of SUCLG2 at residues K93 and K101 affects its stability. **a**, Representative IHC images of the ovaries of bovine with anti-SUCLG2 (n = 3 ovaries per group). Scale bars, 200 μm and 100 μm. **b**,**c**, SUCLG2 protein levels were determined by immunoblot in granulosa cells stably transfected with si-SUCLG2 or si-NC (**b**), overexpressing SUCLG2 or vector (**c**) (n = 3 per group). **d**, The effect of interference or overexpression of SUCLG2 on the viability of GCs was determined by CCK-8, and the quantifications were presented as mean ± SEM of five independent experiments. **e**, The root mean square deviation (RMSD) of the ligand GDP during molecular dynamics simulation in the WT, K93 succinylated, K101 succinylated SUCLG2 model. **f**, The radius of gyration (Rg) of each model is showed during molecular dynamics simulation. **g**, The root mean square fluctuation (RMSF) of each model is showed during molecular dynamics simulation. Statistical analysis was performed using two-tailed Student's t test (**b-d**). $*$ $P < 0.05$, $**$ $P < 0.01$, $***$ $P < 0.001$.

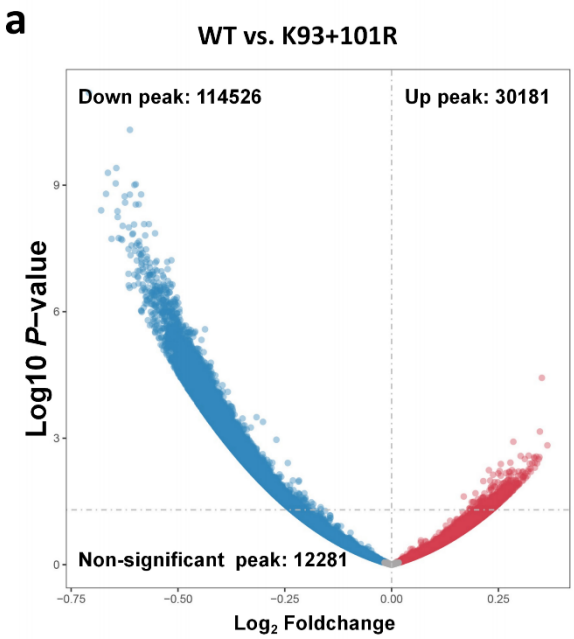

K93+101R vs. WT

Up-regulated GO terms	-Log$_{10}$ *P*
Regulation of autophagy	15.53
Regulation of cell cycle phase transition	11.93
Histone deacetylation	5.09
Ovarian follicle development	2.46
Mitochondrial fission	2.14
Regulation of mitochondrial fusion	1.94

Down-regulated GO terms	-Log$_{10}$ *P*
Wnt signaling pathway	3.82
Regulation of protein catabolic process	3.69
Ubiquitin-protein transferase activator activity	3.21
Histone lysine demethylation	2.89
Cellular response to oxidative stress	2.33
Histone H3-K9 demethylation	1.62

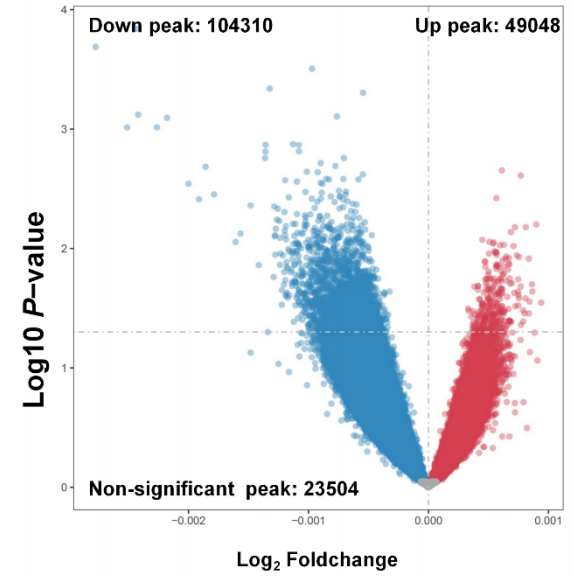

K93+101E vs. K93+101R

Up-regulated GO terms	-Log$_{10}$ *P*
RNA polymerase II-specific DNA-binding transcription factor binding	3.36
Regulation of DNA biosynthetic process	2.39
Negative regulation of organelle organization	1.83
DNA damage response, signal transduction by p53 class mediator	1.58
Chromatin remodeling	1.35
H4 histone acetyltransferase complex	1.33

Down-regulated GO terms	-Log$_{10}$ *P*
Cell fate commitment	5.77
Positive regulation of cellular component biogenesis	4.38
Mitochondrial depolarization	2.68
DNA replication	1.90
Heterochromatin formation	1.85
Positive regulation of DNA repair	1.71

Extended Data Fig. 7|SUCLG2 succinylation affects chromatin binding to histone H4. **a**, Left: Volcano plot of quantified the number of H4K8ac differential binding peaks between WT and SUCLG2$^{K93+101R}$ mutant. Right: The up-regulated or down-regulated peaks enriched Gene Ontology (GO) terms are shown between WT and SUCLG2$^{K93+101R}$ mutant. **b**, Left: Volcano plot of quantified the number of H4K8ac differential binding peaks between SUCLG2$^{K93+101E}$ mutant and SUCLG2$^{K93+101R}$ mutant. Right: The up-regulated or down-regulated peaks enriched Gene Ontology (GO) terms are shown between SUCLG2$^{K93+101E}$ mutant and SUCLG2$^{K93+101R}$ mutant.

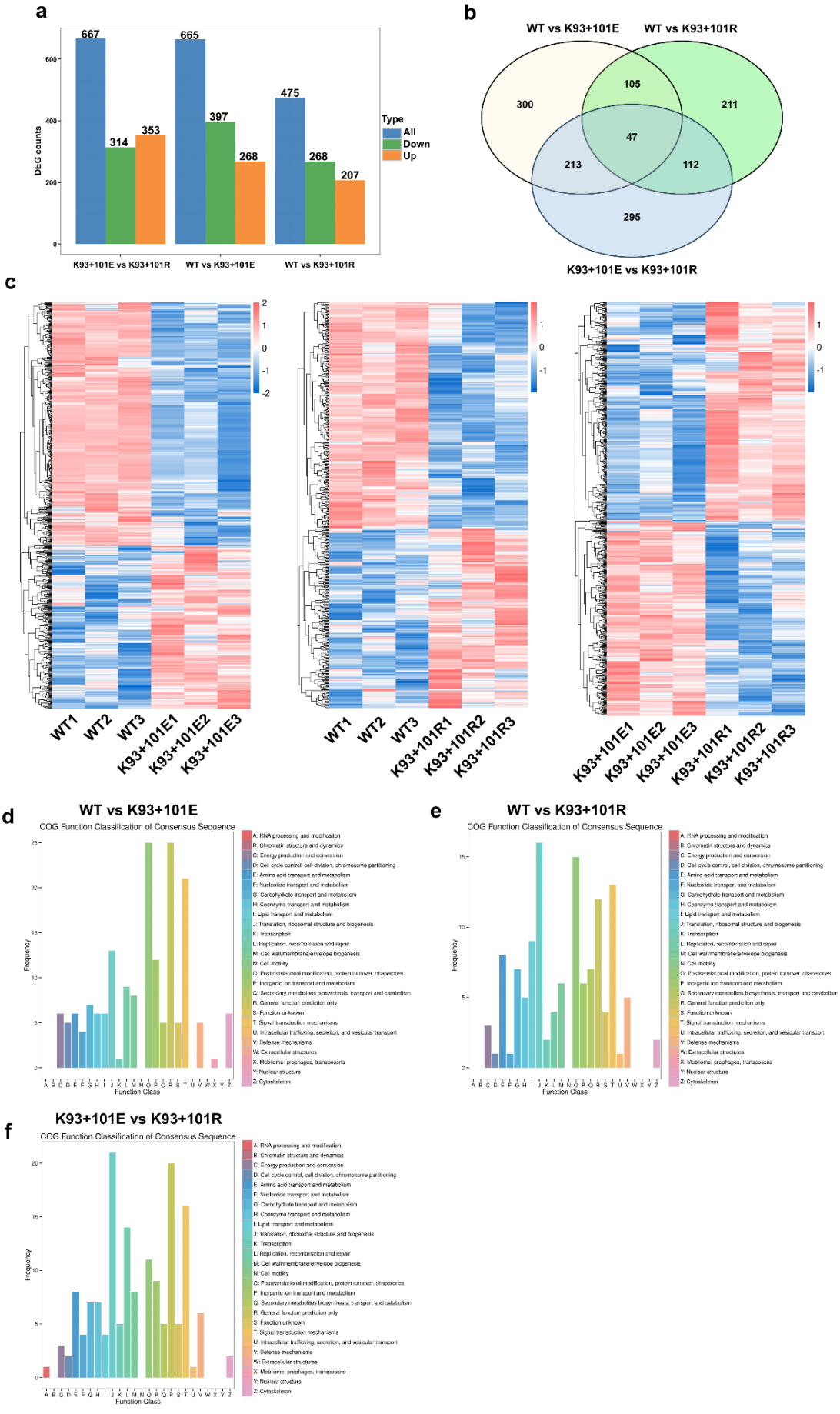
a
DEG counts
Type
All
Down
Up
667
314
353
665
397
268
475
268
207
K93+101E vs K93+101R
WT vs K93+101E
WT vs K93+101R
b
WT vs K93+101E
WT vs K93+101R
300
105
211
47
213
112
295
K93+101E vs K93+101R
c
WT1
WT2
WT3
K93+101E1
K93+101E2
K93+101E3
WT1
WT2
WT3
K93+101R1
K93+101R2
K93+101R3
K93+101E1
K93+101E2
K93+101E3
K93+101R1
K93+101R2
K93+101R3
d
WT vs K93+101E
COG Function Classification of Consensus Sequence
Frequency
Function Class
e
WT vs K93+101R
COG Function Classification of Consensus Sequence
Frequency
Function Class
f
K93+101E vs K93+101R
COG Function Classification of Consensus Sequence
Frequency
Function Class

Extended Data Fig. 8|SUCLG2 succinylation affects gene expression in granulosa cells. **a**, Statistics of differentially expressed genes between each comparison group (n = 3 per group). **b**, The differential genes of different comparison combinations are displayed by Wayne diagram. The numbers in each region represent the number of genes under the corresponding classification, and the overlapping regions represent the number of differential genes shared among the related combinations in this region. **c**, Gene expression clustering heatmaps in different samples. **d-f**, Cluster of orthologous groups (COG) classification statistical analysis of differentially expressed genes between WT vs SUCLG2$^{K93+101E}$ mutant (**d**), WT vs SUCLG2$^{K93+101R}$ mutant (**e**) and SUCLG2$^{K93+101E}$ mutant vs SUCLG2$^{K93+101R}$ mutant (**f**).

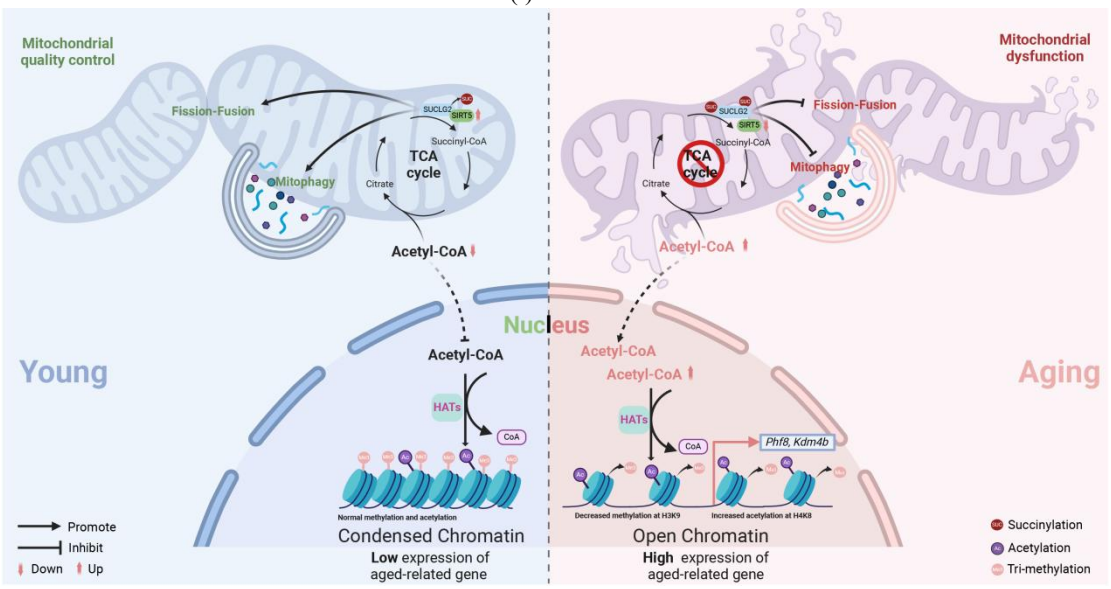

Extended Data Fig. 9|Mechanistic diagram of SIRT5-mediated SUCLG2 desuccinylation in ameliorating ovarian aging. SIRT5 catalyzes desuccinylation of SUCLG2 at K93 and K101 to maintain mitochondrial function and acetyl-CoA homeostasis. Defects in the SIRT5-SUCLG2 axis lead to nuclear acetyl-CoA accumulation, causing aberrant histone H4 hyperacetylation, mitochondrial dysfunction, and subsequent cellular senescence.